

Temporal development of photorefractive solitons up to telecommunication wavelengths in strontium-barium niobate waveguides

M. Wesner,* C. Herden, R. Pankrath, and D. Kip

Fachbereich Physik, Universität Osnabrück, Barbarastrasse 7, D-49069 Osnabrück, Germany

P. Moretti

Laboratoire de Physico-Chimie des Matériaux Luminescents, Université Claude Bernard Lyon 1, 69622 Villeurbanne, France

(Received 5 April 2001; published 29 August 2001)

We experimentally investigate the temporal development of photorefractive solitons in strontium-barium niobate waveguides at visible and infrared wavelengths. The development times in the infrared are shown to be comparable with those in the visible. The results are compared with predictions of a previously published model.

DOI: 10.1103/PhysRevE.64.036613

PACS number(s): 42.65.Tg, 77.84.-s

I. INTRODUCTION

Photorefractive solitons are a new and exceptional topic of the research on photorefractive effects. They can be generated at low power levels of (sub)microwatts [1] and at wavelengths up to $1.5 \mu\text{m}$ [2]. These are parameter regions where other photorefractive effects, such as two-beam coupling [3], are rarely observed, because efficiencies and buildup speeds decrease distinctly. This is different for photorefractive solitons, making their temporal development a highly interesting subject. However, despite the enormous amount of work published on photorefractive steady-state [4,5] and quasi-steady-state solitons [6,7], only a few publications are devoted to time dependencies (see [8,9] and references therein).

Theoretical investigations of the temporal development of photorefractive solitons have been performed by Zozulya and Anderson [10,11] and by Fressengeas *et al.* [12–14]. Experimentally, the self-focusing process, possibly converging into a solitary state, was investigated in the sillenite $\text{Bi}_{12}\text{TiO}_{20}$ [15,16]. Most of the experiments on photorefractive solitons have been performed in the tungsten bronze strontium-barium niobate (SBN) [1,17,18]. Here, however, studies on the temporal development of single-component solitons are still missing.

In this contribution we investigate experimentally the temporal development of photorefractive solitons in planar SBN waveguides at the wavelengths 633, 1047, and 1488 nm. The influence of wavelength, external electric field, and beam intensity on the quasi-steady-state is demonstrated. We compare our measurements with the predictions of the numerical calculations of Fressengeas *et al.* [12–14], and confirm the experimental usefulness of their simplified approach.

II. FUNDAMENTALS

The temporal development of a light beam propagating in a photorefractive medium with an applied external electric

field E_{ext} , neglecting diffusion of charge carriers and photovoltaic fields, can be expressed by [12]

$$i \frac{\partial U}{\partial Z} + \frac{1}{2} \frac{\partial^2 U}{\partial X^2} - \frac{NU}{1+|U|^2} \left[1 - \exp\left(-\frac{t}{\tau_{di}}(1+|U|^2)\right) \right] - N \exp\left(-\frac{t}{\tau_{di}}(1+|U|^2)\right) U = 0. \quad (1)$$

Here, $Z = z/kx_0^2$ and $X = x/x_0$ are the normalized propagation length and transverse length, respectively, where k is the wave vector and x_0 is an arbitrary length. With $U = \mathcal{E}/\sqrt{I_d}$, the electric field amplitude \mathcal{E} is normalized to the square root of $I_d = \sigma_d/\sigma_{ph}^0$, where the dark intensity I_d is defined as the quotient of dark and specific photoconductivity. The time t is normalized to the dielectric relaxation time in the dark, which is determined by crystal properties, $\tau_{di} = \epsilon_0 \epsilon_r / e \mu m$, with e for the elementary charge, ϵ_0 for the vacuum electric permeability, ϵ_r for the static dielectric constant, μ for the electron mobility, and m for the electron density in the dark. The factor N collects important experimental parameters, $N = 2\pi^2 n^4 r_{eff} x_0^2 E_{ext} / \lambda^2$, with n for the linear refractive index of the medium, r_{eff} for the effective electro-optic coefficient, and λ for the light wavelength in vacuum. Obviously, the influence of increasing wavelength on N can be compensated by using a larger external electric field E_{ext} . The partial differential equation can be numerically solved to give the field amplitude U at each time t [19].

Far reaching predictions on the temporal development of solitons were reached by Fressengeas *et al.* [12–14] by assuming a solitary beam shape at each time. Although this condition cannot be strictly fulfilled experimentally, important qualitative evaluations can be carried out with this approach. For a solitary beam, the electric field amplitude can be expressed as

$$U(X, Z, t) = \sqrt{r} \gamma(X, t) \exp(i\nu Z), \quad (2)$$

where γ is the soliton profile normalized by

$$\gamma(0, t) = 1 \quad \text{and} \quad \gamma(\pm\infty, t) = 0. \quad (3)$$

*FAX: (+49) 541 969 3510.

Email address: Monika.Wesner@uos.de

In the Z direction a phase change is allowed by the factor $\exp(i\nu Z)$. The intensity ratio r is determined by the quotient of the beam peak intensity and the dark intensity I_d . Introducing this approach into the wave equation (1) and integrating it using the boundary conditions (3), expressions to determine the soliton profile $\gamma(x)$ at each time are obtained [12]. In the following, we do not investigate the complete soliton profile, but its full width at half minimum (FWHM) w_x .

The conclusions obtained by the approach of Fressengeas *et al.* will be briefly reviewed here.

(1) Following from Eqs. (1) and (2), the soliton's temporal development is determined by three parameters, namely, the intensity ratio r , the parameter $N(\lambda, E_{ext})$, and the dielectric relaxation time in the dark, τ_{di} .

(2) Depending on N and r , some of the curves $w_x(t)$ show a monotonic decrease of w_x , until the steady state is reached. Other curves attain an absolute minimum of the beamwidth during their temporal development before reaching steady state. This minimum is called a quasi-steady-state soliton. Curves showing a quasi-steady-state appear for larger values of r , where the threshold increases with larger N [13].

(3) For a constant value of r , the quasi-steady-state is reached at the same normalized time t/τ_{di} for all N [13].

(4) For constant N , the quasi-steady-state is reached earlier for larger r [14].

(5) From the numerical calculations, the existence of a global normalized time for reaching the steady state is postulated, which is specified by $t/\tau_{di} \approx 3$ [14]. At this time, all curves $w_x(t)$ have reached their steady state, independent of the experimental parameters N and r .

As an example, we display in Fig. 1 the results obtained according to [12,13], using parameters similar to those in our experiment. Shown is the normalized beamwidth w_x/x_0 as a function of the normalized time t/τ_{di} . In Fig. 1(a), the parameter N is kept constant at $N=1.3$, while the intensity ratio r is changed between 0.3 and 40. In Fig. 1(b), the intensity ratio is kept constant at $r=10$, while the parameter N is changed from 0.7 to 3.0. Once the scaling length is chosen, e.g., $x_0 = 10 \mu\text{m}$, N can be attributed to experimental parameters.

III. EXPERIMENTAL METHODS

For our experiments we use y -cut $\text{Sr}_{0.61}\text{Ba}_{0.39}\text{Nb}_2\text{O}_6$ crystals, doped with 0.27 wt% (3000 ppm referred to Nb) of rhodium. The crystal dimensions x, y, z are $4 \times 2 \times 3 \text{ mm}^3$ (used at $\lambda = 633 \text{ nm}$) and $2 \times 2 \times 6 \text{ mm}^3$ (used in the infrared). Here z is the light propagation direction and x is the direction of the crystallographic c axis. Barrier waveguides with a $4.5\text{-}\mu\text{m}$ -thick waveguiding layer were produced by ion implantation [20]. The natural dark intensities of the waveguides are comparatively high, $106 \pm 60 \text{ W/cm}^2$ at $\lambda = 633 \text{ nm}$, $345 \pm 200 \text{ W/cm}^2$ at $\lambda = 1047 \text{ nm}$, and $800 \pm 600 \text{ W/cm}^2$ at $\lambda = 1488 \text{ nm}$. We therefore do not use additional background illumination. The values of the dark intensity are determined by measuring the soliton widths while varying the intensity ratio r [2]. The electro-optic coefficients in the waveguiding layer have been measured before to be

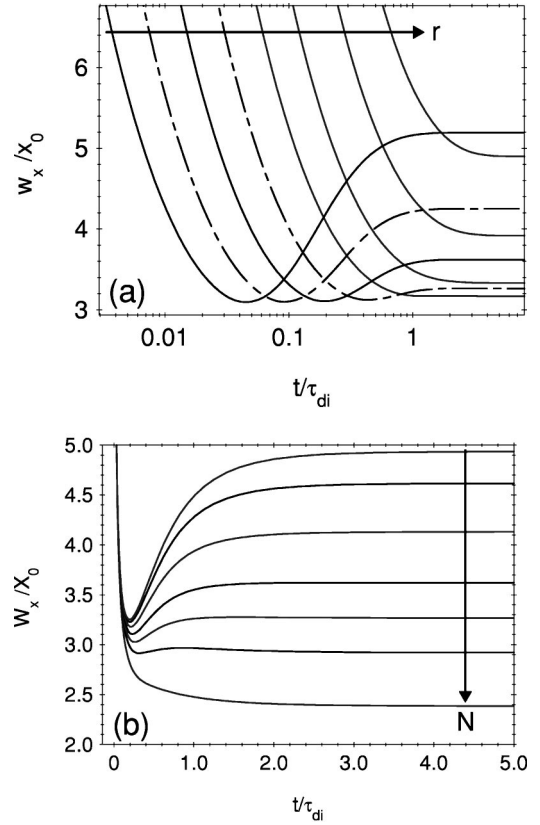


FIG. 1. Normalized soliton width w_x/x_0 as a function of the normalized time t/τ_{di} . (a) $N=1.3$; $r =$ (from left to right) 40, 20, 10, 5, 2.5, 1.3, 0.6, 0.3; (b) $r=10$; $N =$ (from top to bottom) 0.7, 0.8, 1.0, 1.3, 1.6, 2.3, 3.0.

$r_{33} = 148 \pm 7 \text{ pm/V}$ at $\lambda = 633 \text{ nm}$, and $r_{33} = 133 \pm 7 \text{ pm/V}$ at $\lambda = 1047 \text{ nm}$ [2].

In the experiment, an extraordinarily polarized light beam is coupled into the waveguiding layer with the help of a cylindrical and a microscope lens. The aim is to get a nearly collimated beam to achieve an almost constant beam profile along the z direction. In this way, the temporal development along the z direction can be described by a single time constant. Experimentally, we use an approximately $40\text{-}\mu\text{m}$ -wide input beam that has an almost constant width during 6 mm of propagation inside the sample. Especially in the visible wavelength range, this width is rather large when compared to the final soliton width in the steady state. However, we confirmed earlier that in this case “tapered” solitons form inside the crystal, which, after a short propagation inside the crystal, reach their constant solitary profile [2].

The experiment is performed by applying a suitable external electric field parallel to the c axis of the crystal. Then a mechanical shutter is opened and the laser beam is launched into the waveguiding layer. A calibrated charge-coupled device (CCD) camera records the intensity distribution at the crystal's end face, and the beam width w_x FWHM can be evaluated as a function of time. The camera's sampling rate of 25 Hz provides only a limited resolution. However, the use of the CCD camera helps to get rid of problems with the lateral bending of the solitons, especially of the visible wavelengths, which is due to diffusion effects [21].

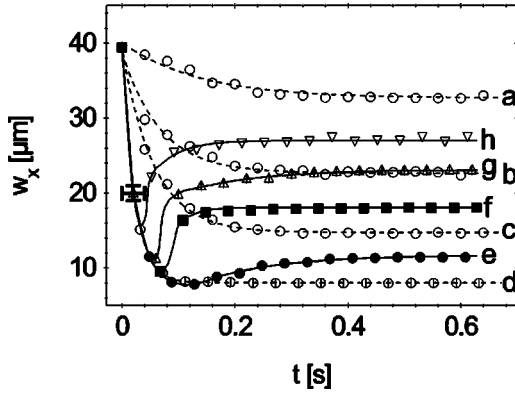


FIG. 2. Temporal development of the soliton width w_x at $\lambda = 633$ nm. External electric field $E_{ext} = 3.25$ kV/cm; steady-state intensity ratio $r =$ (from a to h) 0.08, 0.1, 0.3, 5.3, 10.5, 21, 42, 82. The lines are merely a guide to the eye.

Alternatively, in the infrared, where bending is almost absent, we also use a photodiode with a small aperture to detect the power P_{center} in a small area in the center of the intensity distribution, which is a measure of the beamwidth as well.

IV. EXPERIMENTS AND DISCUSSION

We start our measurements at visible wavelengths ($\lambda = 633$ nm), keeping in a first experiment the external electric field E_{ext} , and thus the parameter N , constant while changing the intensity ratio r . In a second experiment r is kept constant, while E_{ext} is changed.

In Fig. 2 curves $w_x(t)$ for a constant external electric field $E_{ext} = 3.25$ kV/cm are shown for different intensity ratios r . With $x_0 = 10$ μm , $n = 2.28$, and $r_{eff} = 148$ pm/V this results in $N = 6.4$. The steady-state beam intensity is changed between 8.5 W/cm² and 8.7 kW/cm² to give values of r between 0.08 and 82. The steady-state values of the beamwidth w_x show the well known behavior predicted by the soliton's existence curve [4]: The beamwidth first decreases with increasing r , attaining a minimum at $r \approx 3$, and then increases again for larger values of r . Only the curves with larger values of the intensity ratio r show a quasi-steady-state, i.e., a minimum of the beamwidth during the temporal development. Here the minima occur earlier in time for larger r , as predicted by items (2) and (4) of the conclusions obtained by the approach of Fressengeas *et al.*

Next, in Fig. 3 the curves $w_x(t)$ are measured for different external electric fields E_{ext} . From the top to the bottom E_{ext} increases from 2 to 4 kV/cm, and correspondingly the parameter N increases from 4 to 8, using the same parameters as mentioned above. All curves start with an initial beam width $w_0 \approx 40$ μm at $t = 0$. By changing the input power, the output beam peak intensity for each curve is adjusted to about 1 kW/cm² in the steady state, leading to a constant steady-state intensity ratio for all curves of $r \approx 10$. However, it is important to note that during the temporal development the beamwidth and thus the beam intensity change, and therefore also the intensity ratio may differ from the final steady-state value of $r \approx 10$. For smaller values of N the minima that characterize the quasi-steady-state are much

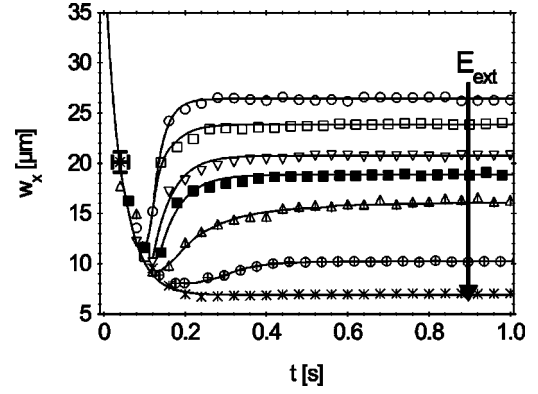


FIG. 3. Temporal development of the soliton width w_x at $\lambda = 633$ nm. Intensity ratio $r \approx 10$, external electric field $E_{ext} =$ (from top to bottom) 2, 2.5, 2.75, 3, 3.25, 3.5, and 4 kV/cm. The lines are merely a guide to the eye.

more pronounced. Within the limited resolution of our measurement, the minima are reached at approximately the same time.

When comparing the experimental curves with the results of the simplified numerical approach in Fig. 1, the qualitative agreement is obvious. Quantitatively, experimental and theoretical curves cover a similar parameter region determined by w_x , N , and r . For instance, comparing Fig. 1(a) and Fig. 2, the experimental values of w_x range from 10 to 40 μm , with $N = 6.4$ and values of r between 0.08 and 82. With $x_0 = 10$ μm , in the theoretical model [Fig. 1(a)] we have beamwidths w_x between 30 and 60 μm , $N = 1.3$, and r changing from 0.3 to 40. The experimental errors in r (on the order of the error in I_d) and E_{ext} (due to, e.g., nonperfect silver paste electrodes) would allow us to choose slightly different values in the numerical calculations, but we do not achieve a better overall coincidence with the experimental data thereby.

Indeed, we cannot expect full quantitative agreement with the rigid assumptions of the numerical approach. First, the medium does not support a soliton in the initial stages of the temporal development ($t \approx 0$), since we start the experiment with broad Gaussian beams. Second, we use an extended medium, while the two-dimensional theoretical approach neglects the z dependence of the beam profile. Third, diffusion effects are not included in the theory, but they do contribute to our experiments at least in the visible wavelength range. Regarding these limitations, the quantitative coincidence is excellent. It demonstrates that the limitation mentioned have no decisive influence. Obviously, the first stages of the temporal development do not differ much for solitary and non-solitary self-focusing [10,11]. Further, the z dependence is moderated by our experimental setup, using nearly collimated initial beams. Last, it has been shown [21] that diffusion effects do not change the beam profile significantly.

With the external electric field kept constant, we next perform similar experiments as in the visible with infrared light, first at the wavelength $\lambda = 1047$ nm. In Fig. 4 the temporal development of the reciprocal power in the beam center, which is proportional to the beamwidth w_x , is shown. We chose an external electric field $E_{ext} = 2.4$ kV/cm. With $x_0 = 10$ μm , $n = 2.26$, and $r_{eff} = 133$ pm/V we obtain $N = 1.5$.

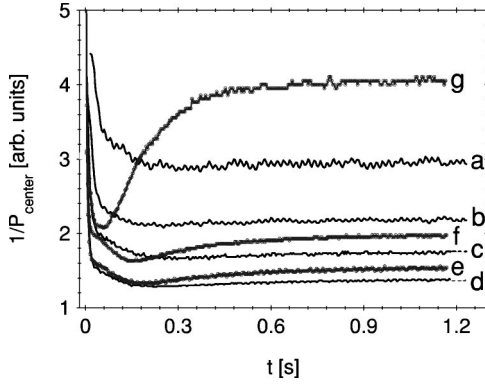


FIG. 4. Temporal development of the power P_{center} in a small area in the beam's center at $\lambda = 1047$ nm. External electric field $E_{ext} = 2.4$ kV/cm; steady-state intensity ratio $r =$ (from a to g) 0.8, 1, 1.4, 1.9, 2.6, 2.8, 5.2.

The output steady-state beam peak intensity is changed between 0.27 and 1.8 kW/cm². Due to the larger value of the dark intensity at $\lambda = 1047$ nm this results in values of r between 0.8 and 5.2. Obviously, a similar temporal behavior can be observed for $\lambda = 1047$ nm as for $\lambda = 633$ nm.

Now we perform the same experiment with available lasers at the wavelengths 1310 and 1488 nm, which are approximately equal to telecommunication wavelengths. The soliton buildup at both wavelengths follows the scheme observed at the smaller wavelengths, as is demonstrated, for example, in Fig. 5 for $\lambda = 1488$ nm. Here we use a constant external electric field $E_{ext} = 8.7$ kV/cm, leading to $N = 2.5$ with $x_0 = 10$ μ m, $n = 2.26$, and $r_{eff} = 125$ pm/V. The beam peak intensity is changed between 0.28 and 0.54 kW/cm², resulting in r between 0.35 and 0.68. Because of the larger dark intensity, it is not possible to reach larger r values with our limited available laser power. However, the tendency to a similar temporal behavior as observed for the other wavelengths can be recognized.

When comparing all measurements, we can indeed find something like a maximum time when all curves $w_x(t)$ have finally reached their steady state. Depending on the chosen convergence range we find that in the 0.27 wt % rhodium-doped waveguides it never takes longer than about 1 s until a steady state is reached. For other dopings, the observed global steady-state times can be distinctly different [22]. Thus these buildup times can be a rough but easy measure for the dielectric relaxation time in the dark. This parameter is rather difficult to measure in a thin waveguiding layer with standard or holographic techniques.

To summarize the influence of larger wavelengths on soliton development, the time to reach the global steady state is

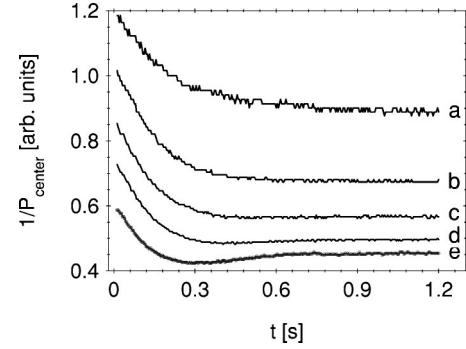


FIG. 5. Temporal development of the power P_{center} in a small area in the beam's center at $\lambda = 1488$ nm. External electric field $E_{ext} = 8.7$ kV/cm; steady-state intensity ratio $r =$ (from a to e) 0.35, 0.4, 0.45, 0.57, 0.68.

mainly determined by the crystal's dielectric relaxation time in the dark, τ_{di} . Regarding the other soliton parameters, namely, r and N , in principle soliton formation should be possible for all values of r and N . However, in practice experimental limitations may occur; for instance, the values of r should not deviate too much from $r \approx 3$ [2]. Here a decrease of N with increasing wavelength can be completely compensated by using larger external electric fields, and the lower intensity ratio r because of the larger dark intensity I_d at longer wavelengths has to be compensated by using beam intensities comparable to the dark intensity.

V. CONCLUSION

In conclusion, for our experimental setup, using nearly collimated initial beams in planar SBN waveguides, the temporal development of the solitons can be qualitatively described by the numerical model of Fressengeas *et al.* [12–14]. The temporal development is thus determined by the intensity ratio r , the parameter $N(E_{ext}, \lambda)$, and the dielectric relaxation time in the dark, τ_{di} . Infrared solitons show a temporal behavior similar that of solitons in the visible; in particular, the buildup times are approximately the same: In the 0.27 wt % rhodium-doped crystals after 1 s at the latest a steady state is reached, independent of the chosen external electric field, the beam intensity, and the wavelength.

ACKNOWLEDGMENTS

The support of the Deutsche Forschungsgemeinschaft, the state of Niedersachsen (Grant No. GRK 695), and the Volkswagen Foundation (Grant No. ZN 1154) is gratefully acknowledged.

- [1] G. Duree, J.L. Schultz, G. Salamo, M. Segev, A. Yariv, B. Crosignani, P. DiPorto, E. Sharp, and R.R. Neurgaonkar, *Phys. Rev. Lett.* **71**, 533 (1993).
 [2] M. Wesner, C. Herden, D. Kip, E. Krätzig, and P. Moretti, *Opt. Commun.* **188**, 69 (2001).

- [3] D.L. Staebler and J.J. Amodei, *J. Appl. Phys.* **43**, 1042 (1972).
 [4] M. Segev, G.C. Valley, B. Crosignani, P. DiPorto, and A. Yariv, *Phys. Rev. Lett.* **73**, 3211 (1994).
 [5] D.N. Christodoulides and M.I. Carvalho, *J. Opt. Soc. Am. B* **12**, 1628 (1995).

- [6] M. Segev, B. Crosignani, A. Yariv, and B. Fischer, *Phys. Rev. Lett.* **68**, 923 (1992).
- [7] B. Crosignani, M. Segev, D. Engin, P. DiPorto, A. Yariv, and G. Salamo, *J. Opt. Soc. Am. B* **10**, 446 (1993).
- [8] W. Krolikowski, B. Luther-Davies, C. Denz, J. Petter, C. Weillnau, A. Stepken, and M. Belic, *Appl. Phys. B: Lasers Opt.* **68**, 975 (1999).
- [9] C. Denz, W. Krolikowski, J. Petter, C. Weillnau, T. Tschudi, M.R. Belic, F. Kaiser, and A. Stepken, *Phys. Rev. E* **60**, 6222 (1999).
- [10] A.A. Zozulya and D.Z. Anderson, *Phys. Rev. A* **51**, 1520 (1995).
- [11] A.A. Zozulya and D.Z. Anderson, *Opt. Lett.* **20**, 837 (1995).
- [12] N. Fressengeas, J. Maufoy, and G. Kugel, *Phys. Rev. E* **54**, 6866 (1996).
- [13] N. Fressengeas, D. Wolfersberger, J. Maufoy, and G. Kugel, *Opt. Commun.* **32**, 414 (1998).
- [14] N. Fressengeas, D. Wolfersberger, J. Maufoy, and G. Kugel, *J. Korean Phys. Soc.* **32**, 414 (1998).
- [15] N. Fressengeas, D. Wolfersberger, J. Maufoy, and G. Kugel, *J. Appl. Phys.* **85**, 2062 (1999).
- [16] D. Wolfersberger, N. Fressengeas, J. Maufoy, and G. Kugel, *Phys. Rev. E* **62**, 8700 (2000).
- [17] M. Segev, B. Crosignani, P. DiPorto, A. Yariv, G. Duree, G. Salamo, and E. Sharp, *Opt. Lett.* **19**, 1296 (1994).
- [18] M.F. Shih, P. Leach, M. Segev, M.H. Garrett, G. Salamo, and G.C. Valley, *Opt. Lett.* **21**, 324 (1996).
- [19] J. Maufoy, N. Fressengeas, D. Wolfersberger, and G. Kugel, *Phys. Rev. E* **59**, 6116 (1999).
- [20] D. Kip, B. Kemper, I. Nee, R. Pankrath, and P. Moretti, *Appl. Phys. B: Lasers Opt.* **65**, 511 (1997).
- [21] M.I. Carvalho, S.R. Singh, and D.N. Christodoulides, *Opt. Commun.* **120**, 311 (1995).
- [22] D. Kip, M. Wesner, V.M. Shandaroy, and P. Moretti, *Opt. Lett.* **23**, 921 (1998).